JACS
JOURNAL OF THE AMERICAN CHEMICAL SOCIETY
Article
pubs.acs.org/JACS

The Chemical Basis of Serine Palmitoyltransferase Inhibition by Myriocin

John M. Wadsworth,[†,#] David J. Clarke,[†,#] Stephen A. McMahon,[‡] Jonathan P. Lowther,[†] Ashley E. Beattie,[†] Pat R. R. Langridge-Smith,[†] Howard B. Broughton,[§] Teresa M. Dunn,[∥] James H. Naismith,[‡] and Dominic J. Campopiano*[,†]

[†]School of Chemistry, The University of Edinburgh, Edinburgh, Scotland, EH9 3JJ, United Kingdom
[‡]Biomedical Sciences Research Complex, The University of St Andrews, Scotland, KY16 9ST, United Kingdom
[§]Molecular Modelling Laboratory, Centro de Investigación Lilly, S.A., 30 28108-Alcobendas, Madrid, Spain
[∥]Department of Biochemistry and Molecular Biology, Uniformed Services University of the Health Sciences, Bethesda, Maryland 20814, United States

Supporting Information

ABSTRACT: Sphingolipids (SLs) are essential components of cellular membranes formed from the condensation of L-serine and a long-chain acyl thioester. This first step is catalyzed by the pyridoxal-5′-phosphate (PLP)-dependent enzyme serine palmitoyltransferase (SPT) which is a promising therapeutic target. The fungal natural product myriocin is a potent inhibitor of SPT and is widely used to block SL biosynthesis despite a lack of a detailed understanding of its molecular mechanism. By combining spectroscopy, mass spectrometry, X-ray crystallography, and kinetics, we have characterized the molecular details of SPT inhibition by myriocin. Myriocin initially forms an external aldimine with PLP at the active site, and a structure of the resulting co-complex explains its nanomolar affinity for the enzyme. This co-complex then catalytically degrades via an unexpected 'retro-aldol-like' cleavage mechanism to a C18 aldehyde which in turn acts as a suicide inhibitor of SPT by covalent modification of the essential catalytic lysine. This surprising dual mechanism of inhibition rationalizes the extraordinary potency and longevity of myriocin inhibition.

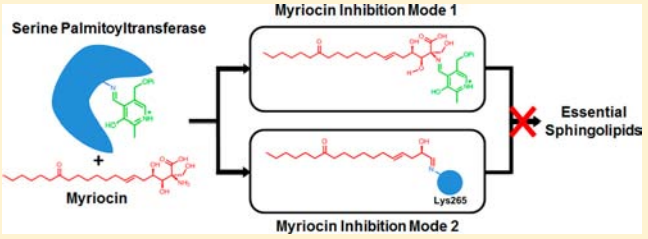

INTRODUCTION

Sphingolipids (SLs) are a large sub class of lipids which are defined by the presence of an amino alcohol functionality of sphingosine (or similar).[1] SLs have been implicated in a wide range of cellular functions and linked to diseases such as diabetes, Alzheimer's, and asthma.[2] Controlling their production is under intense investigation as a new strategy in pharmaceutical therapy. For example, the drug fingolimod, which mimics sphingosine, is used for the treatment of multiple sclerosis and is the first SL-derived therapeutic agent used in the clinic.[3] Serine palmitoyltransferase (SPT, EC 2.3.1.50) is a member of the α-oxoamine synthase (AOS) family of pyridoxal-5′-phosphate (PLP)-dependent enzymes along with 8-amino-7-oxononanoate synthase (AONS),[4] 2-amino-3-ketobutyrate ligase (KBL),[5] 5-aminolevulinate synthase (ALAS),[6] and cholera quorum-sensing autoinducer synthase CqsA.[7] SPT catalyzes the first and rate-determining step in the SL biosynthetic pathway, the decarboxylative, Claisen-like condensation between L-serine (**2**) and an acyl-coenzyme A (CoA) thioester (**4**) to generate the long-chain base intermediate, 3-ketodihydrosphingosine (KDS, **9**, Figure 1). The postulated mechanism involves a number of intermediates including a PLP-bound internal aldimine (**1**, also known as the holo-form), a PLP-L-serine external aldimine (**3**), a quinonoid or masked carbanion (**6**), and a key β-keto acid condensation intermediate (**8**).[8]

Over 160 PLP-dependent enzymes have been characterized,[9] and mechanistic studies of nonspecific PLP inhibitors, such as cycloserine, penicillamine, and β-chloro-alanine,[10] have greatly enhanced the understanding of PLP chemistry as well as highlighting the diversity of reactions that use this organic cofactor as a catalyst. Consequently, PLP-dependent enzymes are now recognized as attractive drug targets.[11] Despite the importance of both PLP enzymes in general and SPT in particular, only a small number of SPT-specific inhibitors have been discovered, all of which are natural products—sphingofungins, viridiofungin A, lipoxamycin, and myriocin (**10**, Figure 1B).[12] Myriocin [(2*S*,3*R*,4*R*,6*E*)-2-amino-3,4-dihydroxy-2-(hydroxymethyl)-14-oxo-6-eicosenoic acid], also known as thermozymocidin and ISP-1, was first discovered in 1972 by two independent groups[13] from the thermophilic molds *Myriococcum albomyces* and *Mycelia sterilia*, and both found the natural product to be a potent antifungal agent. It

Received: June 14, 2013
Published: August 19, 2013

dx.doi.org/10.1021/ja4059876 | J. Am. Chem. Soc. 2013, 135, 14276−14285

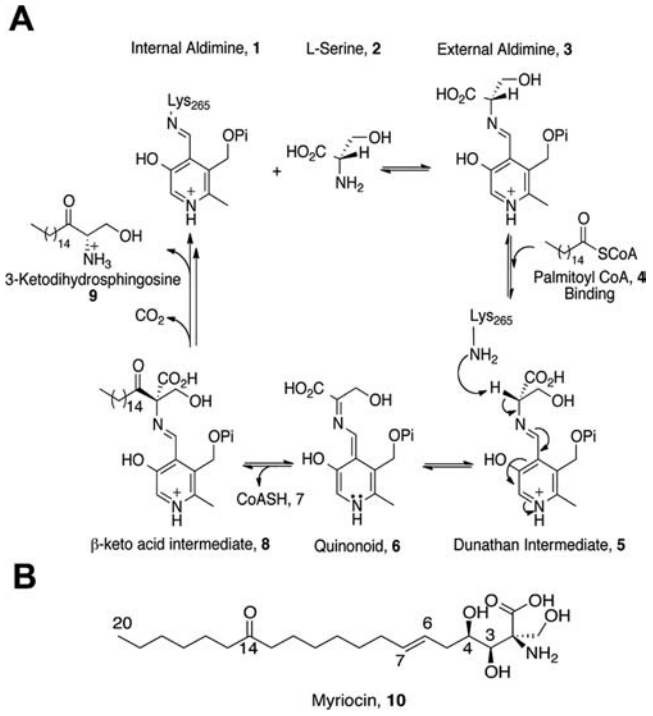

Figure 1. The abbreviated PLP-dependent catalytic mechanism of SPT. (A) The internal aldimine, **1** (holo-SPT) is displaced by L-serine, **2**, to form the external aldimine, **3**. Binding of the second substrate, palmitoyl-CoA, **4**, causes conformational change to give the Dunathan intermediate, **5**. This conformation allows deprotonation of Cα hydrogen by Lys265, forming the quinonoid, **6**. This is followed by nucleophilic attack on the palmitoyl-CoA thioester from Cα, releasing CoASH, **7**, forming the β-keto acid intermediate, **8**. This intermediate undergoes decarboxylation, before release of the product 3-ketodihydrosphingosine (KDS), **9**, and regeneration of the internal aldimine, **1**. (B) The natural product SPT inhibitor myriocin, **10**.

was re-isolated from the fungus *Isaria sinclairii* in 1994 and shown to be a potent immunosuppressant.[14] Kawasaki and colleagues[12d] determined an IC_{50} value of 15 nM, using the mouse cytotoxic T-cell line, CTLL-2 as a model for myriocin-dependent inhibition of cell growth and elimination of ceramide production. Since growth was restored by the addition of sphingosine, it suggested that SPT was the primary target of myriocin. In 1999 Schreiber and colleagues used a myriocin-like affinity resin to identify the two subunits of murine SPT (SPT1 and SPT2 encoded by the genes, *lcb1* and *lcb2*, respectively) as the primary targets of the natural product myriocin.[15]

Myriocin remains the most valuable and widely used chemical probe in SL research; for example, recent studies using the natural product in whole eukaryotic cells and cell extracts have revealed unexpected structural complexity in the membrane-bound SPTs from higher organisms.[2c,16] Despite its use, the molecular basis of myriocin inhibition of SPT is largely unknown. To shed light on the chemistry of this important enzyme−inhibitor complex we have used a soluble, recombinant form of the enzyme from the SL-producing bacterium *Sphingomonas paucimobilis* which has proven an informative model system. Here we present a detailed chemical analysis of the SPT:myriocin inhibition mechanism including a structural description of the covalent PLP:external aldimine of myriocin. We also reveal an unexpected, enzyme-catalyzed myriocin degradation mechanism that generates a second species which acts as a suicide inhibitor of its enzyme target; thus we propose that myriocin acts as a novel dual-mode inhibitor of SPT.

EXPERIMENTAL SECTION

Chemicals and Molecular Biology Tools. Plasmids and competent cells were purchased from Novagen. All buffers and reagents were from Sigma. Palmitoyl-CoA was purchased from Avanti Lipids, and myriocin was purchased from Sigma.

Gene Cloning and Mutagenesis. The *S. paucimobilis* SPT used in this study is in vector pET28a and contains a six histidine tag at the N-terminus. This generates an SPT of 441 amino acids with a short extension at the N-terminus containing the His tag and a 12 amino acid linker. The K265A mutant was made using the Liu mutagenesis protocol[17] with the following primers:

5′-gtcggcactttctct**gcg**tctgttggaactgttggc-3′ (Forward)

5′-acccgccaacagttccaacaga**cgc**agagaaagtgccgac-3 (Reverse)

The bases mutated are shown in bold, and the isolated SPT K265A clone was verified by DNA sequencing. Mass spectrometry analysis of both wild-type and K265A mutant SPTs showed the proteins to be intact with only the N-terminal methionine removed. To avoid confusion and allow comparison with previous data, we number the N-terminally tagged SPT using the same sequence as before.[8] Key active site residues are His159, Asp231, His234, and Lys265.

Expression and Purification of SPT WT and SPT K265A Mutant. Expression and purification of the WT protein has been reported previously.[8] A single colony of pET-28a SPT BL21 (DE3) (or SPT K265A mutant) was used to inoculate 250 mL of LB media with kanamycin (30 μg mL^{-1}) and grown overnight to saturation. This culture was diluted 1:100 in fresh LB/kanamycin and grown to an OD_{600} of 0.6 before expression was induced with 0.1 mM isopropyl β-D-1-thiogalactopyranoside (IPTG). Protein expression continued for 5 h at 30 °C, 200 rpm. Harvested cells where resuspended in lysis buffer 20 mM KPhos, pH 7.5, 150 mM NaCl, 10 mM imidazole, 25 μM PLP and complete protease inhibitor cocktail (Roche) and lysed by sonication (Soniprep 150, 15 cycles of 30 s on followed by 30 s off) on ice. The resulting lysate was centrifuged for 30 min at 47 000 *g*. The supernatant was incubated with Ni resin (Ni-NTA Superflow, Qiagen) for 1 h at 4 °C. The resin was removed and washed, and the protein eluted in lysis buffer supplemented with 300 mM imidazole. Imidazole was removed by dialysis of the protein into 20 mM KPhos, pH 7.5, 150 mM NaCl, 25 μM PLP before a final gel filtration purification step using a Superdex S200 column (GE Healthcare) equilibrated and eluted with 20 mM Tris, pH 7.5, 150 mM NaCl, 25 μM PLP buffer. The purity of the eluted protein was checked by SDS PAGE, and the protein identity confirmed by mass spectrometry.

UV−vis Spectroscopic Measurements. All UV−visible spectra were recorded on a Cary 50 UV−vis spectrophotometer (Varian) and analyzed using Cary WinUV software (Varian). Immediately prior to enzymatic assays, SPT was converted to the holo-form by dialysis against freshly prepared 20 mM KPhos (pH 7.5) containing 150 mM NaCl and 25 μM PLP for 1 h at 4 °C. Excess PLP was removed by passing the protein through a PD-10 (Sephadex G-25M) desalting column (GE Healthcare) before concentration to 40 μM using a VivaSpin 30 kDa cutoff concentration filter. For UV−vis analysis, the concentration of recombinant SPT was 40 μM, and the spectrophotometer was blanked with 20 mM potassium phosphate (pH 7.5) containing 150 mM NaCl. The spectrophotometer was maintained at a constant temperature throughout all time-dependent assays using a Cary PCB-150 single cell Peltier.

SPT Activity Assay. SPT activity was measured using a previously published method that uses a continuous spectrophotometric assay to monitor the release of CoASH from acyl-CoA substrates and reaction with 5,5′-dithiobis-2-nitrobenzoic acid (DTNB).[8b] Assays were performed on a 250 μL scale on a 96-well format in a Biotek Synergy HT plate reader. The enzyme was incubated with L-serine and myriocin in a buffered solution containing DTNB, and the assay was started by the addition of the second substrate, palmitoyl-CoA. The

dx.doi.org/10.1021/ja4059876 | J. Am. Chem. Soc. 2013, 135, 14276−14285

CoASH thiol product was monitored by observation of the TNB^- anion at 412 nm (ε_{max} = 14 150 M^{-1} cm^{-1}) for 45 min. A typical experiment contained 0.2 μM SPT, 20 mM L-serine, 250 μM palmitoyl-CoA, and 0.2 mM DTNB in 100 mM HEPES, pH 8.0. Kinetic constants were calculated using GraphPad Prism 6 software. K_m and competition experiments were performed and calculated using Michaelis–Menten kinetics.

Inhibition Studies. Due to the tight binding nature of myriocin, it was necessary to calculate inhibition kinetics using the regimen described by Williams and Morrison.[18] The Michaelis–Menten equation can not be used as the assumption that the free inhibitor concentration is equal to the total inhibitor concentration is not valid; instead the K_i is calculated using the quadratic Morrison equation. The K_m for L-serine was calculated from rates measured with increasing concentrations of L-serine (0.1–40 mM) while maintaining the palmitoyl-CoA concentration at 250 μM in excess of its K_m (35 μM). Similarly, the K_m for palmitoyl-CoA was calculated from rates measured with increasing concentrations of palmitoyl-CoA (2.5–1500 μM) and excess L-serine (20 mM).

In order to determine the type of inhibition between SPT and myriocin, IC_{50} values for the inhibitor were determined in the presence of a number of different substrate concentrations (both L-serine and palmitoyl-CoA). During these experiments the enzyme concentration remained fixed at 200 nM. In order to ensure solubility of myriocin in the assay mixture, myriocin was dissolved in DMSO then diluted to its final desired concentration with the DMSO concentration at less than or equal to 1%. For the experiments varying palmitoyl-CoA concentration it was necessary to add L-ser and palmitoyl-CoA prior to addition of myriocin. The resulting IC_{50} values were plotted against substrate concentrations in a manner described by Cha, Williams and Morrison.[19] All kinetic experiments were performed in triplicate.

To determine the reversibility of inhibition, 40 μM SPT was treated with 200 μM myriocin and incubated for either 10 min or 16 h at 25 °C. Excess inhibitor was then removed by extensive dialysis against 20 mM KPhos, pH 7.5, 150 mM NaCl, with 25 μM fresh PLP. Aliquots were then removed at specific time points and assayed for SPT activity as above.

Mass Spectrometry. All mass spectra were acquired using a 12 Telsa SolariX Fourier transform ion cyclotron resonance mass spectrometer equipped with an electrospray ion source (Bruker Daltonics). Liquid chromatography mass spectrometry (LC-MS) experiments were performed using an Ultimate 3000 HPLC system (Dionex).

For the detection of the PLP-myriocin aldimine (**11**) and the PLP-decarboxymyriocin aldimine (**15**), samples were prepared by incubating myriocin (200 μM) with either wild-type or K265A SPT (40 μM) at 25 °C. At specific time points, aliquots were removed and analyzed by LC-MS using a Phenomenex C18 Aeris Widepore 50 × 2.1 mm column, operating at a flow rate of 150 μL/min. A gradient of 2–98% acetonitrile was performed over 20 min. In order to preserve the acid labile imine bond, no acidic modifiers were added to either mobile phase. For single ion monitoring, the mass resolving quadrupole was set to a specific m/z, with a 10 m/z window, and ions were typically accumulated for 2000 ms.

For intact protein mass spectrometry, LC-MS was performed using a monolithic PS-DVB (500 μm x 50 mm) reverse-phase analytical column (Dionex). Protein (100 pmoles) was loaded onto the column (maintained at 60 °C) followed by a 10 min linear gradient from 2 to 95% acetonitrile (flow rate 20 μL/min). Mass spectra were collected every 200 ms between m/z 600 and 2500. Data analysis was performed using DataAnalysis software (Bruker Daltonics). Neutral spectra were created using maximum entropy deconvolution.

Peptide Mass Mapping. For peptide mass mapping, SPT (40 μM) was treated with 200 μM myriocin. Derivitization was allowed to proceed for 18 h at 25 °C, while being monitored by UV–vis spectroscopy. After loss of the peak at 430 nm in the UV–vis spectrum, the sample was chemically reduced by treatment with 10 mM $NaBH_4$. Finally, this sample was treated with the protease trypsin (Promega, sequence grade) for 18 h at 37 °C at an enzyme:protein ratio of ~1:20 by weight. The resulting peptide mixture was analyzed by LC-MS using a monolithic PS-DVB (500 μm × 50 mm) reverse-phase analytical column (Dionex). The column was maintained at 60 °C, and a linear gradient of 5–70% acetonitrile was performed over 30 min.

The resulting data was analyzed by DataAnalysis software (Bruker Daltonics). A mass list was created using the SNAP 2.0 algorithm (Bruker Daltonics) and searched against the known primary sequence of SPT using the MS-Fit software (University of California). For data searching, error tolerances were set to 10 ppm.

Structural Biology. Protein for crystallization was concentrated to 20 mg mL^{-1} and incubated with 5 equiv of myriocin immediately prior to crystallization trials. Crystals of K265A SPT were grown by vapor drop diffusion at 20 °C over the course of 2 weeks and are readily reproducible. The optimum growth conditions are 32% PEG MME 2000, 0.1 M HEPES pH 7.5, and a protein:precipitant ratio of 1:1. Prior to data collection the crystals were cryo-cooled in mother liquor doped with 20% glycerol. Data were collected at Beamline I04-1 at the Diamond synchrotron light source, Oxfordshire, England, and processed in an automated manner using Xia2.[20] The structure was solved by molecular replacement using PHASER[21] and PDB code 2JG2 as a model. The myriocin dictionary was created using PRODRG.[22] The model was refined using REFMAC5[23] with TLS. COOT[24] was used for manual manipulation of the structure and model quality was assessed throughout with MOLPROBITY.[25] Data collection and refinement statistics can be found in Table S2.

RESULTS

Formation of a PLP-Myriocin Aldimine in Wild-Type SPT. Holo-SPT (**1**) displays a characteristic UV–vis spectrum for a PLP-containing protein with absorption maxima at 333 and 420 nm (Figure 2A), corresponding to the equilibrium between the ketoenamine and enolimine forms of PLP.[8b] Addition of 5-fold molar excess of myriocin to holo-SPT led to an immediate increased absorbance with a maximum at 430 nm and loss of the 333 nm peak as previously observed by Ikushiro et al.[12b] Hanada et al. proposed that this species corresponds to a PLP-myriocin aldimine (**11**) formed as a result of transimination (Figure 2B) that acts as a stable mimic of the β-keto acid intermediate (**8**) in the SPT mechanism (Figure 1).[26] LC electrospray ionization (ESI)-MS analysis detects a species of monoisotopic mass 631.30153 Da consistent with the PLP-myriocin aldimine (**11**) (predicted monoisotopic mass 631.29902 Da; $[(C_{29}H_{47}N_2O_{11}P) + H]^+$) (Figure 2C). Attempts to trap the reduced form of (**11**) using $NaBH_4$ were unsuccessful.

Using the method by Cha,[19a] IC_{50} values for the inhibitor were determined at fixed enzyme concentrations while systematically varying each substrate concentration. IC_{50} values increase linearly with varying L-serine and palmitoyl-CoA concentration, establishing myriocin as a competitive inhibitor for both L-serine and palmitoyl-CoA substrates (Figure S1). The Morrison equation,[19b] yields a K_i for myriocin of 967 ± 98 nM (Figure 2D).

PLP-Myriocin Inhibitory Complex Undergoes Slow Catalytic Degradation. The PLP-myriocin aldimine (**11**) at 25 °C was stable for 90 min before a slow spectral transition took place over 16 h (decrease at 430 nm and a concomitant increase at 331 and 400 nm) (Figure 3A); indicating conversion of **11** to a previously unseen PLP aldimine. To our surprise the new species remained catalytically compromised, indicating the new PLP aldimine is also inhibitory. Immediately after addition of myriocin only 7.7% of enzyme activity remains (as expected); however after complete conversion (judged by no further change in the UV–vis spectrum) activity remained low at 10.1% relative to the starting value (Figure 3B). Lowering the

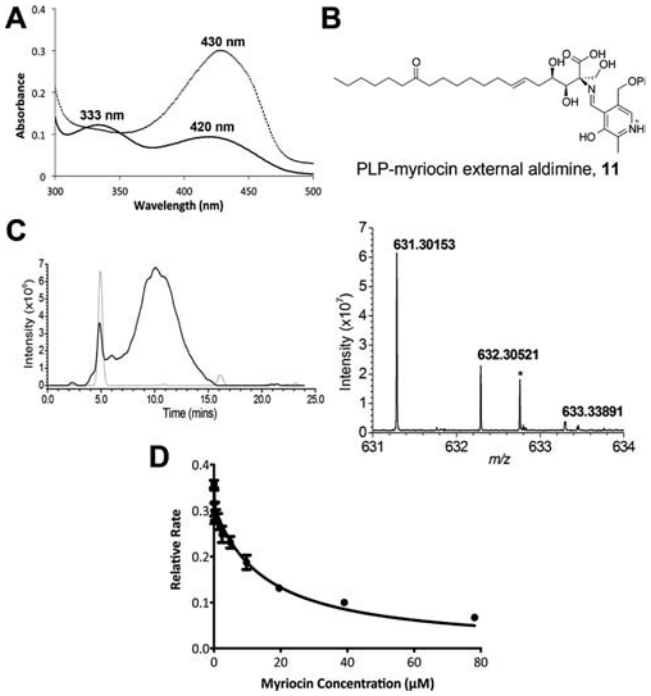

Figure 2. SPT inhibition occurs via formation of a PLP-myriocin aldimine. (A) UV−vis spectrum of 40 μM SPT before (solid line) and after 200 μM myriocin addition (dotted line). (B) The proposed structure of the inhibitory complex, a PLP-myriocin aldimine, **11**. (C) Detection of the PLP-myriocin aldimine by LC-MS. Top: extracted ion chromatogram at m/z 631. Bottom: high-resolution mass spectrum of the PLP-myriocin aldimine, obtained by summing the spectra between t = 8−12 min. ($[M + H]^+$ $C_{29}H_{48}N_2O_{11}P$; predicted m/z 631.29902; observed error 4.0 ppm). * denotes a contaminant. (D) Inhibition of SPT by myriocin, data fitted using the Morrison equation. The K_i obtained for the PLP-myriocin aldimine is 967 ± 98 nM.

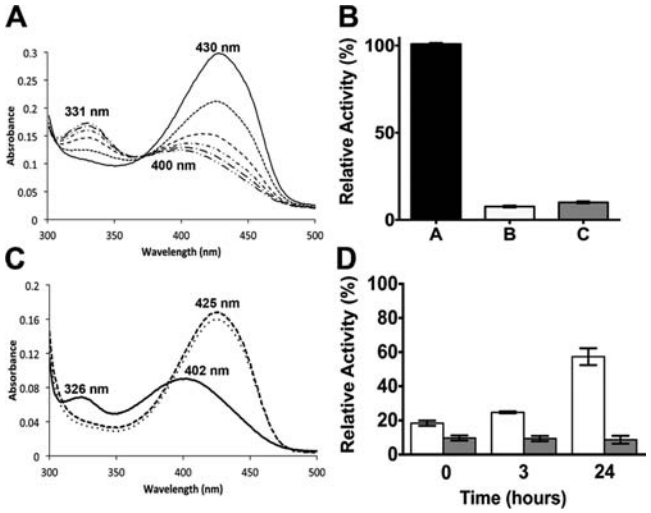

Figure 3. The PLP-myriocin aldimine undergoes SPT-catalyzed degradation to form a second inhibitory species. (A) UV−vis analysis of the degradation of the PLP-myriocin external aldimine in wild-type SPT. The PLP-myriocin external aldimine (solid line) is stable for 90 min, before a decrease at 430 nm is observed, which is accompanied by a concomitant increase at 331 and 400 nm over 16 h (dotted and dashed lines). (B) Relative activity of wild-type SPT after incubation with myriocin. A, wild-type SPT activity (100%); B, wild-type SPT activity after 10 min incubation with 200 μM myriocin (7.7%); C, wild-type SPT activity after 16 h incubation with 200 μM myriocin (10.1%). (C) UV−vis analysis of SPT K265A (40 μM) showed two absorbance maxima at 326 and 402 nm (solid line). Upon addition of 200 μM myriocin, an immediate shift to a single peak at 425 nm occurred (dotted line), indicating the formation of a PLP-myriocin aldimine complex. Over 16 h this spectrum remains unchanged (dashed line), indicating that the PLP-myriocin aldimine complex is not degraded by this mutant enzyme. (D) Relative enzymatic activity after removal of inhibiting species by dialysis. SPT was inhibited with 200 μM myriocin and incubated for 10 min (white bars) or 16 h (gray bars) at 25 °C before removal of myriocin by extensive dialysis. The enzymatic activity was then determined at 0, 3, and 24 h after dialysis.

temperature to 4 °C arrested the decomposition of the PLP-myriocin aldimine (Figure S2). Interestingly, a catalytically inactive mutant, SPT K265A, displayed two peaks with λ_{max} values of 326 and 402 nm, consistent with PLP bound noncovalently as the aldehyde (Figure 3C). Upon incubation with 5-fold molar excess of myriocin we observed a large shift to a single absorbance maximum at 425 nm similar to that observed in the wild-type SPT. In contrast to the wild-type incubation this spectrum remained unchanged over 16 h at 25 °C indicating a stable PLP-myriocin external aldimine. Taken together, these intriguing observations suggest that the initial SPT:PLP-myriocin inhibitor complex breaks down to form a second species that also inhibits SPT.

To test the reversibility of inhibition we first generated the SPT:PLP-myriocin complex by incubation of SPT with the inhibitor for 10 min and 16 h at 25 °C. After this incubation period the temperature was lowered to 4 °C to stop further conversion and extensive dialysis against buffer containing 25 μM fresh PLP was performed for 24 h. Aliquots were removed from the dialysate at specific time points (0, 3, and 24 h) and assayed for SPT activity (Figure 3D). For the enzyme incubated with myriocin for the shorter time (10 min) and then dialyzed for 3 h, no significant activity was recovered; however, dialysis for 24 h recovered 60% enzymatic activity (Figure 3D, white bars). This regain in enzymatic activity was also accompanied by a change in the UV−vis spectrum back to the internal aldimine form, i.e., λ_{max} 333 and 420 nm (data not shown). Taken together, this data from short, 10 min incubations of SPT with myriocin is consistent with the formation of an initial enzyme−inhibitor complex which is noncovalent in nature and reversible, albeit with a very slow off rate (k_{off}). Thus this analysis supports our assignment of the PLP-myriocin aldimine (**11**) as the initial inhibitory species. In contrast, for the enzyme preincubated with myriocin for 16 h, no detectable regain in activity was observed after dialysis either at 3 or 24 h (Figure 3D, gray bars), indicating that this second, newly formed species acts as an irreversible inhibitor of SPT.

SPT-Catalyzed Myriocin Degradation Occurs via a 'Retro-Aldol-Like' Mechanism. Our spectroscopic and kinetic observations, coupled with a detailed understanding of the mechanism of SPT and other PLP-dependent enzymes,[7] allowed us to consider possible breakdown mechanisms of the SPT:PLP-myriocin complex. We postulated that a slow, "retro-aldol-like" process occurs during prolonged enzyme−inhibitor incubations (Figure 4). To test this hypothesis we used mass spectrometry analysis to attempt the detection of the low molecular weight products of the reaction. Unfortunately, using several derivatization methods (Girard's reagent T; 2,4-dinitrophenylhydrazine), we were unable to capture the putative long chain octadecenal product (**12**).

The reason for this became clear after intact protein mass spectrometry analysis of the SPT:myriocin reaction after 16 h

dx.doi.org/10.1021/ja4059876 | J. Am. Chem. Soc. 2013, 135, 14276−14285

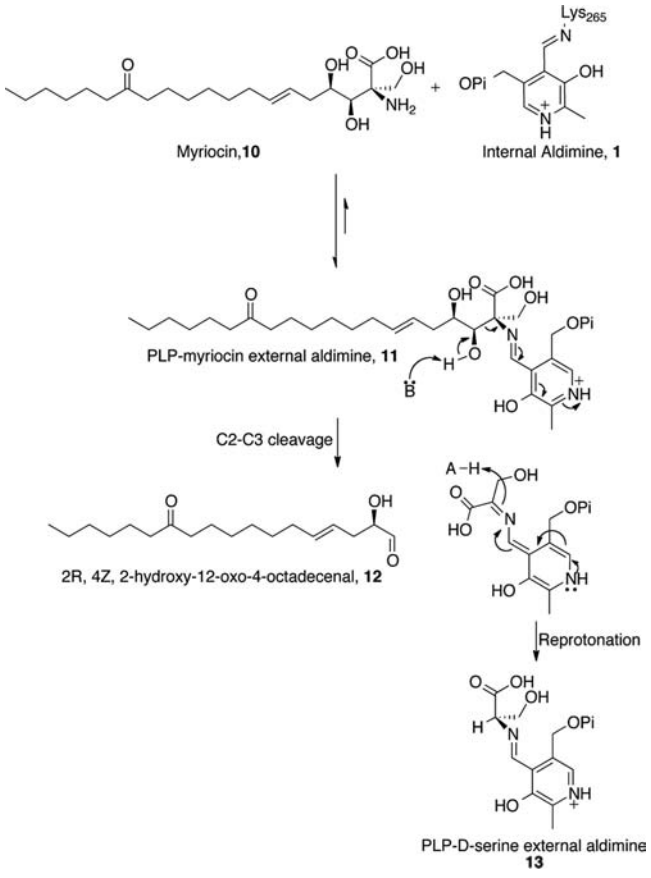

Figure 4. The proposed "retro-aldol-like"mechanism for the observed degradation of the PLP-myriocin aldimine. Myriocin, **10**, undergoes fast transamination with the internal aldimine, **1**, releasing Lys265 and forming the PLP-myriocin aldimine inhibitory complex, **11**. This inhibitory complex is slowly degraded by deprotonation of the myriocin C_3-hydroxyl, with C2−C3 bond cleavage and movement of electrons into the pyridine ring of PLP. This results in the formation of a 2-hydroxyl-C_{18} aldehyde species, **12**, and a PLP-D-serine aldimine, **13**.

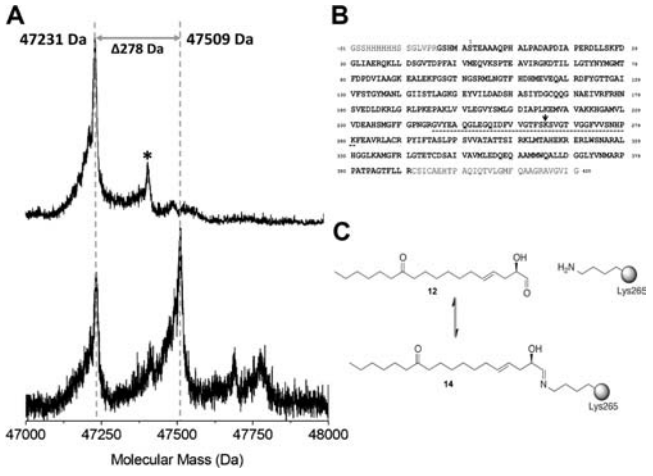

Figure 5. Mass spectrometry analysis of the myriocin-derived covalent modification of SPT. (A) Intact protein mass spectrometry of SPT (40 μM) before (top) and after (bottom) 16 h treatment with 200 μM myriocin at 25 °C. SPT displays an average neutral mass of 47 231 Da. After myriocin treatment a prominent new species of average mass 47 509 is observed (Δmass +278 Da). Minor peaks highlighted by * arise from α-*N*-gluconoylation of the His-tag. (B) Sequence coverage achieved when analyzing myriocin-modified SPT enzyme. Amino acids highlighted in bold were observed in the peptide mass fingerprint (see also Table S1). The myriocin-derived modification was isolated to a single site between Glu245 and Lys280 (underlined); this sequence contains a single internal lysine residue, Lys265 (highlighted by the arrow). (C) The myriocin-derived modification displayed a Δmass +282.24 Da (after hydride reduction; see also Figure S4), this is consistent with condensation of the C18-aldehyde (**12**) onto the amine of Lys265 forming the imine (**14**), with subsequent chemical reduction of the imine and ketone functional groups ($+C_{18}H_{34}O_2$).

incubation at 25 °C (Figure 5). We detected a covalent adduct of SPT (**14**) with a mass matching that of the wild-type enzyme modified by a condensation with the predicted octadecenal (**12**) (47 509 Da, Δmass +278 Da, Figure 5A). This condensation product (**14**) was susceptible to $NaBH_4$ reduction which led to an increase in mass of the adduct by 4 Da (47 513 Da, Figure S3); consistent with chemical reduction of a covalent SPT-octadecenal imine adduct as well as reduction of the ketone at position 12 of the carbon chain in (**14**). Peptide mass fingerprinting identified Lys265 as the site of modification (Figure 5B and Table S1). After trypsin digest and MS analysis, three peptide species were observed which displayed monoisotopic masses consistent (within error 4 ppm) with Lys265 modified by Δmass +282.24 Da ($+C_{18}H_{34}O_2$) (Figure S4). This observation of a myriocin-derived adduct at Lys265 of SPT provides convincing evidence for our proposed retro-aldol-like breakdown of the PLP-myriocin aldimine to a reactive product which selectively covalently modifies an essential residue in SPT. The formation of this adduct also accounts for the irreversible nature of inhibition observed during prolonged SPT:myriocin incubations.

Structure of a SPT K265A:PLP-Myriocin External Aldimine Complex. We were unable to prepare crystals of the wild-type SPT:PLP-myriocin aldimine complex, most likely due to aldimine degradation. However crystals of SPT K265A were obtained that diffracted to 1.6 Å resolution and contained a canonical dimer in the asymmetric unit (Figure 6A). The mobility/flexibility of the acyl chain prevented us from assigning a structure beyond carbon 9 of myriocin. Nevertheless difference electron density revealed a PLP-myriocin aldimine complex had formed (Figure 6B). The myriocin stereochemistry is retained: the *Z* configuration of the double bond at position C6 and *cis* diol geometry at positions C3 and C4. We were surprised to discover that the density indicates that myriocin had undergone loss of the carboxylate from the C2 position to form a PLP-decarboxymyriocin aldimine (**15**). We built the model reasoning the replacement of the carboxylate with a proton (sp^3 hybridized carbon), but the resolution on its own is not sufficient to distinguish an sp^3 from an sp^2 carbon (Figure 6B). As had been noted previously[8b] residues from both SPT subunits are involved in PLP binding, and the active site is at the dimer interface (Figure 6C).

Comparison of this complex with the wild-type SPT:PLP-L-serine external aldimine complex (PDB code 2W8J)[8b] reveals essentially the same positioning of the PLP rings in both structures (Figure 6D). Moreover, many key active site residues (His159, Asp231, His234) adopt similar positions. However Arg378, which is involved in a key electrostatic interaction with the carboxylate of L-serine in the SPT:PLP-L-serine external aldimine structure, is swung out of the active site with concomitant change in the important mobile loop 378 RPPATP 383; both the loop and Arg378 are partially disordered in the new complex. These changes are the result

dx.doi.org/10.1021/ja4059876 | J. Am. Chem. Soc. 2013, 135, 14276−14285

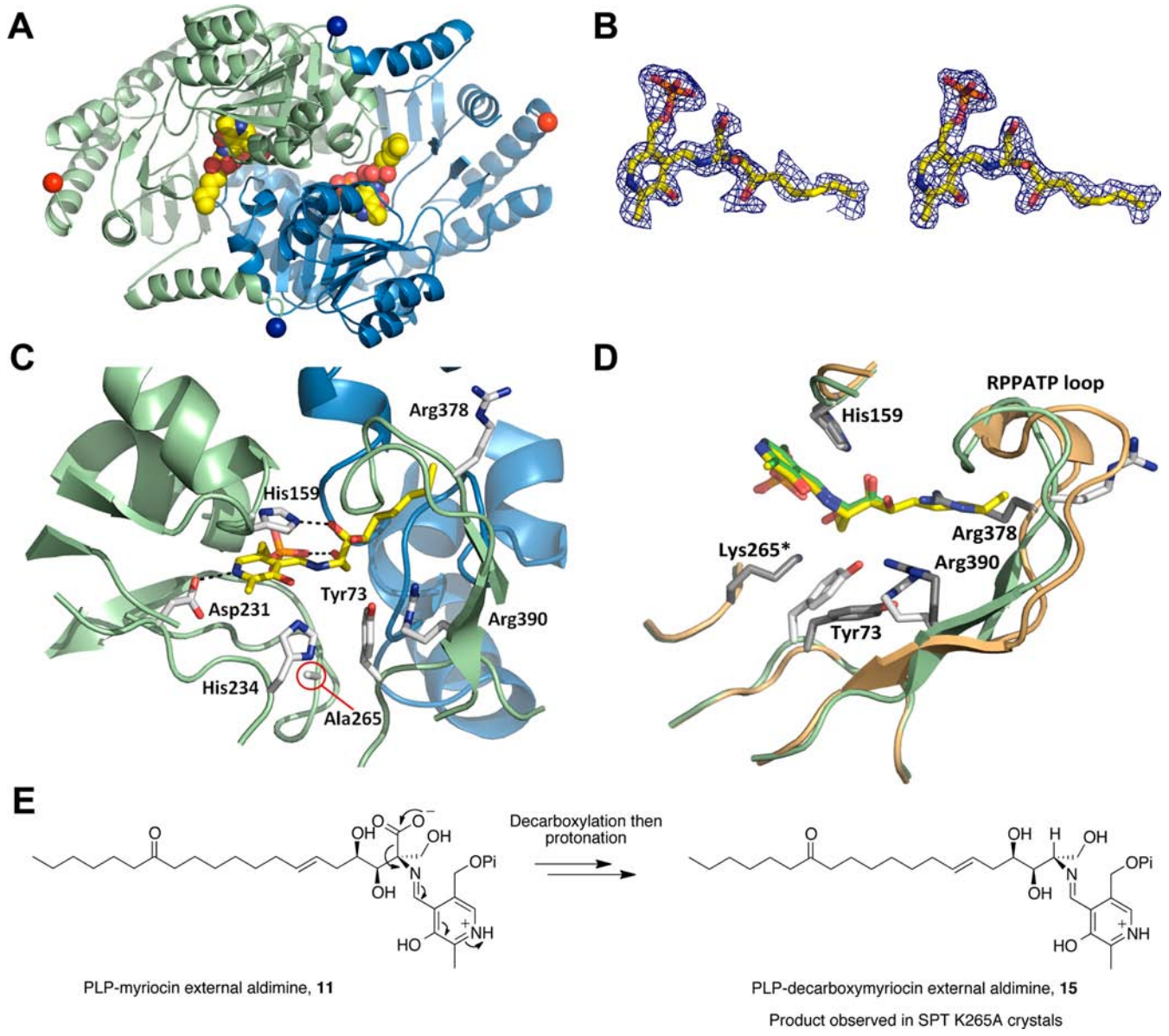

Figure 6. The structure of SPT K265A PLP-decarboxymyriocin aldimine inhibitory complex. (A) The biological SPT dimer of the decarboxylated myriocin complex. The protein is shown as a cartoon with one subunit colored pale green and the other pale blue. The PLP external aldimine of the decarboxylated myriocin (**15**) is shown in space fill with carbons colored yellow, nitrogen blue, phosphorus orange. The N terminii are marked as dark-blue spheres and C-terminii as red spheres. (B) Left: the F_o-F_c map (blue chicken wire contoured at 1.8σ, carve radius 1.5 Å) calculated from a model which had never contained either PLP or myriocin. Atoms are colored as in (A). Right: the final F_o-F_c map contoured at 0.85σ with a carve radius 1.8 Å. (C) Detailed representation of the active site interactions, carbon atoms are colored yellow and shown in sticks for the PLP-decarboxymyriocin aldimine **15**. Carbon atoms in protein side chains are shown as white sticks, others atoms are colored as in (A). The hydrocarbon chain of the myriocin inserts into a hydrophobic pocket. (D) Superposition of the PLP-decarboxymyriocin external aldimine (colored as before) with the PLP-L-serine external aldimine 2W8J (cartoon pale orange, protein side chain carbons dark gray, aldimine carbons colored green, other atoms are colored as before). The key catalytic Lys265 residue is mutated to Ala in the decarboxylated myriocin complex. (E) Decarboxylation mechanism to account for PLP-decarboxymyriocin external aldimine observed in the crystal structure of SPT K265A.

of accommodating the extended hydrophobic tail of **15**. We also note that Arg390, a conserved residue which is required for product formation in the SPT catalytic cycle,[27] adjusts its side chain conformation and makes interactions with both Tyr73 and the C4 hydroxyl of myriocin. In the experimental maps the aromatic portion of the side chain of Tyr73 is not visible in the experimental density despite other plausible conformations being precluded by packing. We confirmed by DNA sequencing and mass spectrometry that the residue was tyrosine.

DISCUSSION

Natural products and their derivatives are responsible for over half of all Food and Drug Administration (FDA)-approved drugs[28] and continue to provide excellent lead molecules.[29] Natural products also serve as excellent chemical probes that can be used to tease out the fine details of biochemical pathways and networks.[30] Myriocin, as well as possessing potent antifungal, antibacterial, and immune suppression activity, is also a valuable chemical tool. Recently Breslow et al. used myriocin to probe the multiprotein, membrane-bound

dx.doi.org/10.1021/ja4059876 | J. Am. Chem. Soc. 2013, 135, 14276−14285

SPT complex (denoted SPOTs) from the endoplasmic reticulum (ER) of yeast that contains LCB1, LCB2, TSC3P, ORM proteins and Sac1 phosphatase.[2c] The SPOTs complex is now known to be central to SL biosynthesis in higher organisms acting as a metabolic rheostat.[31] SLs are now recognized as important in the etiology of many significant human diseases. The pro-drug fingolimod, 2-amino-2-[2-(4-octylphenyl)ethyl]propane-1,3-diol, becomes phosphorylated and mimics sphingosine 1-phosphate (S1P) in the body. The drug suppresses the immune system and is used in the treatment of relapsing remitting multiple sclerosis where it is thought to work by binding to S1P receptors. There is now widespread interest in regulating the production of SLs in the body, and the most obvious target is the SPOTs complex which contains SPT. There are two related obstacles to progress: first the human SPOTs complex is not currently tractable to biochemical study, and there is very limited understanding of how the exemplar inhibitor myriocin works at a molecular level. To overcome these obstacles we have employed the bacterial SPT homologue to reveal the molecular details of myriocin inhibition for the first time.

We have experimentally confirmed the existence of the previously assumed SPT:PLP-myriocin external aldimine inhibitor complex (**11**) by mass spectrometry and spectroscopy (Figure 2). We observed that myriocin (K_i 967 nM) was a potent competitive inhibitor for both L-serine and palmitoyl-CoA, an observation consistent with the ordered, bi-bi mechanism of AOS enzymes and the inhibitor acting as a intermediate mimic. Despite this nanomolar potency, we were unable to completely abolish the activity of the enzyme, and our data suggest that this is because at the concentration of the enzyme required for reliable assay, we cannot dissolve sufficient myriocin to saturate the binding site. *In vivo*, with endogenous SPT levels (found within an ER-bound, SPOTs complex) where the enzyme is in a hydrophobic lipid environment, this limitation is not expected to occur. The Schiff's base external aldimine formed between PLP and myriocin (**11**) is analogous to that formed between PLP and D-serine, a known, but weak, SPT inhibitor.[32] This inhibition should be reversible by incubation with fresh PLP which would displace the inhibitor and restore the holo, internal aldimine form. Indeed, this was the case, but only if the PLP was added to the enzyme:inhibitor complex relatively soon after it was formed. However, addition of PLP could not rescue the enzyme if the SPT:PLP-myriocin complex was subjected to prolonged incubation.

Coupled to this surprising result regarding the kinetics we also observed interesting, time-dependent spectroscopic changes of the SPT:PLP-myriocin external aldimine complex (**11**). This suggested to us that this initial complex was breaking down to an unanticipated second inhibitory species. We generated an inactive SPT (K265A) by removal of the key, conserved active site lysine which not only binds the PLP but also plays an essential role in acid/base catalysis during the mechanism. The SPT K265A mutant binds PLP (albeit noncovalently) and forms the PLP-myriocin external aldimine **11**, but it does not undergo the apparent breakdown observed with the wild-type enzyme suggesting Lys265 is crucial for this enzyme-catalyzed reaction. Mass spectrometry and chemical reduction establishes that in the wild-type SPT the PLP-myriocin external aldimine converts to a C18 imine adduct of Lys265, the key catalytic residue. This covalent modification results in irreversible inhibition of SPT that cannot be rescued by incubation with PLP. This result was entirely unexpected and suggested both a previously unsuspected catalytic activity of SPT as well as a novel duel mechanism of action of SPT inhibition by myriocin.

We were unable to obtain crystals of the wild-type enzyme with myriocin in the active site presumably because the PLP-myriocin aldimine degrades during the two week time scale of crystallization. However, the catalytically inactive K265A mutant did allow us to capture an external aldimine complex, but even then the refined structure revealed that it had undergone a surprising decarboxylation leaving a PLP-decarboxymyriocin aldmine **15** in the active site. To investigate the time-scale of this decarboxylation process, we used mass spectrometry analysis of the SPT K265A:myriocin incubation and found that the PLP-myriocin aldimine (**11**) is stable at room temperature for at least seven days with decarboxylation only observed to occur after this time (Figure S5).

PLP is a versatile cofactor that can use the electron sink properties of the protonated pyridine ring to catalyze a wide range of reactions of amino acid substrates including racemization and decarboxylation.[33] These different chemical reactions proceed from the same key, PLP-amino acid external aldimine and are controlled by the architecture of the particular enzyme active site. Dunathan put forward a hypothesis that outlined the stereoelectronic constraints that govern PLP-dependent enzymes.[34] Modeling the SPT K265A PLP-myriocin external aldimine complex (**11**) places the carboxylate perpendicular to the PLP ("Dunathan conformation") that would allow decarboxylation by the mechanism proposed in Figure 6E. However, its extreme slowness relative to *bone fide* PLP-dependent decarboxylases cautions that the PLP-myriocin aldimine in K265A is not optimally aligned for this reaction. It is worth noting here that the precise orientation of the PLP-myriocin aldimine required for decarboxylation may not be achievable to the wild-type enzyme. In the wild-type SPT the side chain of K265 would be very close to/clash with the carboxylate, perhaps distorting it out of the Dunathan conformation or stabilizing the carboxylate by an ionic interaction. In our previous study of the SPT:PLP-L-serine external aldimine complex of *S. paucimoblis* SPT we revealed that the carboxylate group is held in a specific orientation by salt bridges with Arg378 and His159.[8b,27] In this arrangement decarboxylation is not favored, rather deprotonation of the L-serine at Cα by K265 is achieved only upon a conformational change caused by palmitoyl-CoA binding (Figure 1).[8b,35]

An overlay of the wild-type PLP-L-serine and the K265A PLP-decarboxymyriocin structures reveals that the configuration of the SPT active site remains relatively well conserved (Figure 6D) as well as providing a molecular insight into why myriocin is a nanomolar inhibitor (Figure S6a). Conserved residues His159, Asp231, and His234 are all in the same relative positions within the active site. Moreover, the CH_2OH headgroup of myriocin interacts with the 5′-phosphate of PLP in the same manner as the hydroxyl group from L-serine (Figure S6B). Of key note, the 3,4 *cis* diol of decarboxymyriocin makes hydrogen bonds to the protein, notably the 3-hydroxy of myriocin with the important catalytic residue His159; this interaction would be expected to be preserved in the wild-type SPT:myriocin complex. The hydrogen-bond network that surrounds and includes the 4-hydroxy of decarboxymyriocin may be changed by the presence of Lys265, but at least some of the same network seems certain to persist and this too involves the same residues that interact with the carboxylate of the PLP-L-serine external aldimine. These interactions rationalize the

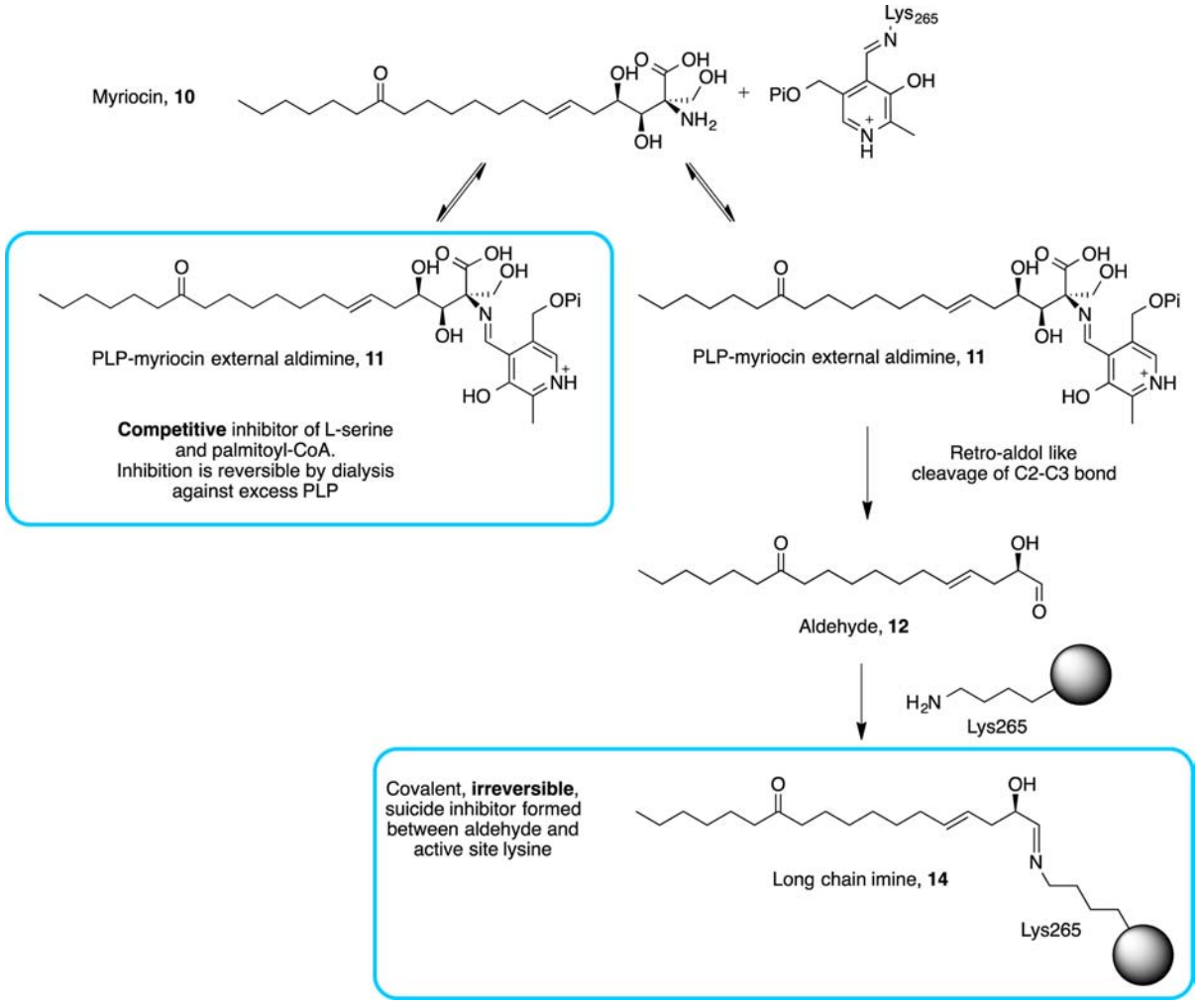

Figure 7. Summary of myriocin's dual mode of action. Inhibitory species highlighted in boxes. Left: myriocin reacts with PLP in the active site to form the inhibitory PLP-myriocin aldimine **11**, this species is stable for greater than 1 h at physiological temperature with inhibition being reversible upon addition of excess PLP. Right: PLP-myriocin aldimine **11** decomposes over 16 h, at physiological temperature, to produce a long chain aldehyde (**12**) that reacts with the active site lysine to form an imine, thus rendering the enzyme inactive. This covalent modification can be classed as suicide inhibition.

competitive inhibition with L-serine. Accompanying these interactions are movements of the side-chains of Tyr73, Arg378, and Arg390 as well as a displacement of a key conserved stretch of amino acids (RPPATP) that constitute a mobile loop that undergoes conformational changes during the catalytic cycle. The 6,7 *trans* double-bond geometry of myriocin is clearly defined, and we can see electron density for the carbon chain up to C9 which sits in the hydrophobic cleft adjacent to PLP. The carbon tail of myriocin binds in a similar orientation to the decanoyl-tail of the PLP-product external aldimine observed bound in the crystal structure of the related AOS enzyme CqsA from *Vibrio cholera* (Figure S7)[7] consistent with our hypothesis that myriocin mimics the condensation intermediate.

The structure also rationalizes the unexpected retro-aldol degradation of the PLP-myriocin external aldimine **11** into the C18 aldehyde **12**. This mechanism requires a base to abstract the proton from the 3-hydroxy of myriocin. Based on its role in the SPT reaction and the fact that a K265A mutant was unable to catalyze the retro-aldol myriocin degradation, Lys265 was a prime candidate for this role. However, structural overlay suggests that Lys265 would be on the wrong face to perform this role (Figure 6D). However, the absolutely conserved His159 is positioned 2.6 Å away from the 3-hydroxy of myriocin, and we propose that it initiates the breakage of the C2−C3 bond with the electrons sinking into the PLP ring (Figures 4 and S6A). Unfortunately, it is difficult to test this hypothesis using site-directed mutagenesis at this position since Ikushiro and colleagues showed that SPT His159 mutants are catalytically compromised enzymes that favor abortive transamination of L-serine.[36] With respect to the role of Lys265 during the retro-aldol reaction, we favor a mechanism in which it protonates the resulting formal carbanion at C2, acting as an acid. This would explain why the K265A mutant does not catalyze the retro-aldol reaction. Again we caution the slowness of the reaction indicates that the enzyme is not optimally arranged for this catalysis, although it does occur over a time scale that we monitored spectroscopically. Having carried out this chemistry, the deprotonated lysine is perfectly positioned to attack the newly formed C18 aldehyde species (**12**) to form a covalent aldimine adduct (**14**) (Figure 7). Such a hydrophobic C18 molecule would be predicted to slowly dissociate and thus favor imine formation over release from the enzyme. Since this second inhibitor modifies the key catalytic lysine

dx.doi.org/10.1021/ja4059876 | J. Am. Chem. Soc. 2013, 135, 14276−14285

residue irreversibly, it will block access to the active site and prevent regeneration by PLP on a biologically relevant time scale. Indeed, we show that the enzyme remained inhibited by this species 72 h after extensive dialysis. The observed stability of the long chain imine (**14**) may well be due to the presence of the alpha hydroxyl, which will allow tautomerization to the α-aminoketone via the amino-enolate.

CONCLUSION

We set out to delineate the structural and mechanistic details of how myriocin inhibits SPT, and in doing so we have revealed unexpected and hitherto unprecedented chemistry (summarized in Figure 7). Our results demonstrate that, as predicted, myriocin acts as a classical intermediate mimic inhibitor with nanomolar affinity for its target. However, once bound in the active site the inhibitory species is broken down by the enzyme to generate a reactive product which acts a suicide inhibitor by covalent modification of a key active site residue conserved in all SPTs.

The PLP-catalyzed retro-aldol reaction that breaks down the myriocin calls to mind other important PLP-dependent enzymes that use the cofactor to catalyze C−C bond cleavage. Serine hydroxymethyltransferase,[37] which is involved in one carbon metabolism, and CqsA,[7] which produces quorum sensing molecules, both use a proposed retro-aldol mechanism to generate glycine from L-serine and L-threonine, respectively. Furthermore, the proposed mechanism for myriocin degradation is reminiscent of the mechanism of the PLP-dependent sphingosine-1-phosphate (S1P) lyase (S1PL), the terminal enzyme of SL biosynthesis that catalyzes the breakdown of S1P.[38] During the catalytic cycle of S1PL, the C3 hydroxyl group of the key PLP-S1P external aldimine is deprotonated, which leads to C2−C3 bond cleavage and production of hexadecenal and phosphoethanolamine. The similarity of the long chain aldehyde product of S1PL to the suicide-inhibitor produced by SPT-catalyzed breakdown of myriocin, **12**, is striking. This suggested to us a possible feedback mechanism whereby the end product of the SL pathway, hexadecenal, may regulate SL biosynthesis by inhibiting SPT, the enzyme that catalyzes the first step in *de novo* SL synthesis. Indeed, in preliminary *in vitro* studies, we have found that hexadecanal inhibits SPT with an IC_{50} of 144 μM (Figure S8).

The high sequence homology between the SPTs from bacteria and other higher order species suggests that the mechanism of myriocin inhibition is conserved, and studies on the human enzyme are underway. The unprecedented combination of tight binding and mechanism-based inactivation within a single molecule described herein has the potential to inform the design of a new class of inhibitors for SPT and other PLP-dependent enzymes.

ASSOCIATED CONTENT

Supporting Information

(S1) Determination of the mode of action between SPT by the inhibitor myriocin. (S2) The UV−vis spectral transitions observed upon prolonged incubations of SPT with myriocin. (S3) Mass spectra showing the chemical reduction of the covalent adduct formed by prolonged incubation of SPT with myriocin. (S4 and Table S1) Peptide mass mapping confirming the location of the SPT modification at Lys265 after prolonged incubation with myriocin. (S5) Mass spectrometry analysis of the products of the reaction between SPT K265A and myriocin. (S6) Schematic representation of the SPT K265A PLP-decarboxymyriocin complex and the PLP phosphate-binding cup. (S7) Overlay of the SPT active site geometry of the PLP-decarboxymyriocin external aldimine structure with the *V. cholera* CqsA enzyme with the trapped product external aldimine bound. (S8) Dose response curve showing SPT inhibition by hexadecanal. X-ray crystal structure data collection and refinement statistics can be found in Table S2. This material is available free of charge via the Internet at http://pubs.acs.org.

AUTHOR INFORMATION

Corresponding Author

dominic.campopiano@ed.ac.uk

Author Contributions

[#]These authors contributed equally.

Notes

The authors declare no competing financial interest.

ACKNOWLEDGMENTS

We wish to thank the BBSRC for awarding grants to D.J.C. (BB/I013687/1) and J.H.N. (BB/F009739/1) that support D.J.C./J.P.L. and S.A.McM., respectively. J.M.W. is supported by a joint Ph.D. studentship between the University of Edinburgh and Lily pharmaceuticals. A.E.B. is supported by a joint Ph.D. studentship between the University of Edinburgh and The Derek Stewart Charitable Trust. The collaboration between D.J.C. and T.M.D. is supported by BBSRC grant (BB/G53045X/1). Protein Data Bank (PDB): The crystallographic data for the SPT-PLP:decarboxymyriocin structure is deposited under accession code 4BMK.

REFERENCES

(1) (a) Pruett, S. T.; Bushnev, A.; Hagedorn, K.; Adiga, M.; Haynes, C. A.; Sullards, M. C.; Liotta, D. C.; Merrill, A. H. *J. Lipid Res.* **2008**, *49* (8), 1621−1639. (b) Merrill, A. H. *Chem. Rev.* **2011**, *111* (10), 6387−6422.

(2) (a) Summers, S. A.; Nelson, D. H. *Diabetes* **2005**, *54* (3), 591−602. (b) van Echten-Deckert, G.; Walter, J. *Prog. Lipid Res.* **2012**, *51* (4), 378−393. (c) Breslow, D. K.; Collins, S. R.; Bodenmiller, B.; Aebersold, R.; Simons, K.; Shevchenko, A.; Ejsing, C. S.; Weissman, J. S. *Nature* **2010**, *463* (7284), 1048−1053.

(3) Yeung, B. K. S. *Curr. Opin. Chem. Biol.* **2011**, *15* (4), 523−528.

(4) Webster, S. P.; Alexeev, D.; Campopiano, D. J.; Watt, R. M.; Alexeeva, M.; Sawyer, L.; Baxter, R. L. *Biochemistry* **2000**, *39* (3), 516−528.

(5) Schmidt, A.; Sivaraman, J.; Li, Y.; Larocque, R.; Barbosa, J. A. R. G.; Smith, C.; Matte, A.; Schrag, J. D.; Cygler, M. *Biochemistry* **2001**, *40* (17), 5151−5160.

(6) Astner, I.; Schulze, J. O.; van den Heuvel, J.; Jahn, D.; Schubert, W.-D.; Heinz, D. W. *EMBO J.* **2005**, *24* (18), 3166−3177.

(7) Jahan, N.; Potter, J. A.; Sheikh, M. A.; Botting, C. H.; Shirran, S. L.; Westwood, N. J.; Taylor, G. L. *J. Mol. Biol.* **2009**, *392* (3), 763−773.

(8) (a) Yard, B. A.; Carter, L. G.; Johnson, K. A.; Overton, I. M.; Dorward, M.; Liu, H.; McMahon, S. A.; Oke, M.; Puech, D.; Barton, G. J.; Naismith, J. H.; Campopiano, D. J. *J. Mol. Biol.* **2007**, *370* (5), 870−886. (b) Raman, M. C. C.; Johnson, K. A.; Yard, B. A.; Lowther, J.; Carter, L. G.; Naismith, J. H.; Campopiano, D. J. *J. Biol. Chem.* **2009**, *284* (25), 17328−17339.

(9) Raboni, S.; Spyrakis, F.; Campanini, B.; Amadasi, A.; Bettati, S.; Peracchi, A.; Mozzarelli, A.; Contestabile, R.; Lew, M.; Hung-Wen, L. Pyridoxal 5′-Phosphate-Dependent Enzymes: Catalysis, Conformation, and Genomics. In *Comprehensive Natural Products II*; Elsevier: Oxford, 2010; pp 273−350.

(10) (a) Lowther, J.; Yard, B. A.; Johnson, K. A.; Carter, L. G.; Bhat, V. T.; Raman, M. C. C.; Clarke, D. J.; Ramakers, B.; McMahon, S. A.; Naismith, J. H.; Campopiano, D. J. *Molecular BioSystems* **2010**, *6* (9), 1682−1693. (b) Lowther, J.; Beattie, A. E.; Langridge-Smith, P. R. R.; Clarke, D. J.; Campopiano, D. J. *MedChemComm* **2012**, *3* (8), 1003−1008. (c) Badet, B.; Roise, D.; Walsh, C. T. *Biochemistry* **1984**, *23* (22), 5188−94.
(11) (a) Conti, P.; Tamborini, L.; Pinto, A.; Blondel, A.; Minoprio, P.; Mozzarelli, A.; De Micheli, C. *Chem. Rev.* **2011**, *111* (11), 6919−6946. (b) Amadasi, A.; Bertoldi, M.; Contestabile, R.; Bettati, S.; Cellini, B.; di Salvo, M. L.; Borri-Voltattorni, C.; Bossa, F.; Mozzarelli, A. *Curr. Med. Chem.* **2007**, *14* (12), 1291−324.
(12) (a) Fujita, T.; Hirose, R.; Yoneta, M.; Sasaki, S.; Inoue, K.; Kiuchi, M.; Hirase, S.; Chiba, K.; Sakamoto, H.; Arita, M. *J. Med. Chem.* **1996**, *39* (22), 4451−4459. (b) Ikushiro, H.; Hayashi, H.; Kagamiyama, H. *Biochemistry* **2004**, *43* (4), 1082−1092. (c) Hanada, K.; Nishijima, M.; Fujita, T.; Kobayashi, S. *Biochem. Pharmacol.* **2000**, *59* (10), 1211−1216. (d) Miyake, Y.; Kozutsumi, Y.; Nakamura, S.; Fujita, T.; Kawasaki, T. *Biochem. Biophys. Res. Commun.* **1995**, *211* (2), 396−403.
(13) (a) Kluepfel, D.; Bagli, J.; Baker, H.; Charest, M. P.; Kudelski, A. *Jpn. J. Antibiot.* **1972**, *25* (2), 109−15. (b) Aragozzini, F.; Manachini, P. L.; Craveri, R.; Rindone, B.; Scolastico, C. *Tetrahedron* **1972**, *28* (21), 5493−5498.
(14) Fujita, T.; Inoue, K.; Yamamoto, S.; Ikumoto, T.; Sasaki, S.; Toyama, R.; Chiba, K.; Hoshino, Y.; Okumoto, T. *Jpn. J. Antibiot.* **1994**, *47* (2), 208−15.
(15) Chen, J. K.; Lane, W. S.; Schreiber, S. L. *Chemistry & Biology* **1999**, *6* (4), 221−235.
(16) Han, S.; Lone, M. A.; Schneiter, R.; Chang, A. *Proc. Natl. Acad. Sci. U.S.A.* **2010**, *107* (13), 5851−5856.
(17) Liu, H.; Naismith, J. *BMC Biotechnol.* **2008**, *8* (1), 1−10.
(18) Williams, J. W.; Morrison, J. F., [17] The kinetics of reversible tight-binding inhibition. In *Methods Enzymol.*, Daniel, L. P., Ed. Academic Press: Waltham, MA, 1979; Vol. *63*, pp 437−467.
(19) (a) Cha, S. *Biochem. Pharmacol.* **1975**, *24* (23), 2177−2185. (b) Williams, J.; Morrison, J. *Meth. Enzymol.* **1979**, *63*, 437−467.
(20) Winter, G. *J. Appl. Crystallogr.* **2010**, *43* (1), 186−190.
(21) McCoy, A. J.; Grosse-Kunstleve, R. W.; Adams, P. D.; Winn, M. D.; Storoni, L. C.; Read, R. J. *J. Appl. Crystallogr.* **2007**, *40* (Pt 4), 658−674.
(22) Schuttelkopf, A. W.; van Aalten, D. M. F. *Acta Crystallogr., Sect. D: Biol. Crystallogr.* **2004**, *60* (8), 1355−1363.
(23) Winn, M. D.; Isupov, M. N.; Murshudov, G. N. *Acta Crystallogr., Sect. D: Biol. Crystallogr.* **2001**, *57* (Pt 1), 122−33.
(24) Emsley, P.; Cowtan, K. *Acta Crystallogr., Sect. D: Biol. Crystallogr.* **2004**, *60* (Pt 12 Pt 1), 2126−32.
(25) Davis, I. W.; Leaver-Fay, A.; Chen, V. B.; Block, J. N.; Kapral, G. J.; Wang, X.; Murray, L. W.; Arendall, W. B., 3rd; Snoeyink, J.; Richardson, J. S.; Richardson, D. C. *Nucleic Acids Res.* **2007**, *35* (Web Server issue), W375−83.
(26) Hanada, K. *Biochim. Biophys. Acta, Mol. Cell Biol. Lipids* **2003**, *1632* (1−3), 16−30.
(27) Lowther, J.; Charmier, G.; Raman, M. C.; Ikushiro, H.; Hayashi, H.; Campopiano, D. J. *FEBS Lett.* **2011**, *585* (12), 1729−1734.
(28) (a) Newman, D. J.; Cragg, G. M. *J. Nat. Prod.* **2012**, *75* (3), 311−35. (b) Swinney, D.; Anthony, J. *Nat. Rev. Drug Discovery* **2011**, *10*, 507−519. (c) Schulze, C. J.; Bray, W. M.; Woerhmann, M. H.; Stuart, J.; Lokey, R. S.; Linington, R. G. *Chem. Biol.* **2013**, *20* (2), 285−95.
(29) (a) Jesse, W.-H. L.; Vederas, J. C. *Science* **2009**, *325* (5937), 161−165. (b) Fischbach, M. A.; Walsh, C. T. *Science* **2009**, *325* (5944), 1089−1093.
(30) Carlson, E. E. *ACS Chem. Biol.* **2010**, *5* (7), 639−653.
(31) Tafesse, F. G.; Holthuis, J. C. M. *Nature* **2010**, *463* (7284), 1028−1029.
(32) Hanada, K.; Hara, T.; Nishijima, M. *FEBS Lett.* **2000**, *474* (1), 63−65.
(33) Eliot, A. C.; Kirsch, J. F. *Annu. Rev. Biochem.* **2004**, *73* (1), 383−415.
(34) Dunathan, H. C. *Proc. Natl. Acad. Sci. U.S.A.* **1966**, *55* (4), 712−716.
(35) Ikushiro, H.; Fujii, S.; Shiraiwa, Y.; Hayashi, H. *J. Biol. Chem.* **2008**, *283* (12), 7542−7553.
(36) Shiraiwa, Y.; Ikushiro, H.; Hayashi, H. *J. Biol. Chem.* **2009**, *284* (23), 15487−15495.
(37) Florio, R.; di Salvo, M. L.; Vivoli, M.; Contestabile, R. *Biochim. Biophys. Acta, Proteins Proteomics* **2011**, *1814* (11), 1489−1496.
(38) Bourquin, F.; Capitani, G.; Grutter, M. G. *Protein Sci.* **2011**, *20* (9), 1492−508.